

Formation flying in Space-Borne Artificial Magnetic Dipole Field

By Yu CHENG,^{1),(2)} Gerard GÓMEZ,^{1),(2)} Josep J. MASDEMONT³⁾ and Jianping YUAN^{1),†}

¹⁾School of Astronautics, Northwestern Polytechnical University, Xi'an, China

²⁾IEEC & Department de Matemàtiques i Informàtica, Universitat de Barcelona, Barcelona, Spain

³⁾IEEC & Department de Matemàtiques, Universitat Politècnica de Catalunya, Barcelona, Spain

In this paper, we consider a new dynamical scenario in which a constantly charged spacecraft (follower) moves near a leader spacecraft, which follows a circular Keplerian orbit around the Earth and generates a rotating artificial magnetic dipole. Considering three general orientations of the dipole: normal, radial and tangential, we study the dynamics of the system and its application potential in formation flying. For this purpose, the critical points of the system and their stabilities are explored, the different families of periodic orbits around each equilibrium point are computed, as well as the stability, possible bifurcations and terminations (if exist). By selecting suitable periodic orbits, two formation flying configurations are briefly explored, in which satellites are placed at the periodic orbits around two or four symmetric equilibrium points of the system.

Key Words: Relative Dynamics, Periodic Orbits, Invariant Tori, Lorentz force, Formation Flying

Nomenclature

$\frac{q}{m}$: charge-to-mass ratio
 β : angular ratio

Subscripts

n : normal case
 r : radial case
 t : tangential case

1. Introduction

The Lorentz force perturbation on the charged spacecraft by geomagnetic field was firstly studied by Hough,¹⁾ then the concept of Lorentz Augmented Orbit(LAO) was introduced by Peck,⁴⁾ which, afterwards has drawn more and more attention. A charged spacecraft experiences Lorentz force while moving in a magnetic field, the propellantlessness of Lorentz force offers more advantage than the traditional chemical propulsion, and makes it a promising meaning for space missions.

Previous work mainly focused on the natural magnetic fields, such as geomagnetic field²⁾ or other planetary magnetic field.⁵⁾ Plenty of applications of LAO have been studied, such as new synchronous orbits by the geomagnetic Lorentz force,⁶⁾ formation flying^{7), 16)} Jovian orbit insertion⁸⁾ and Gravity-Assist manoeuvre.⁹⁾ Several control strategies have been considered for different kinds of relevant missions¹⁰⁾¹¹⁾¹²⁾.

Vokrouhlicky 1989

With regard to the artificial magnetic field, Kong¹³⁾ introduced the idea of Electro-Magnetic Formation Flight(EMFF), which uses the intersection between the electromagnetic field of several satellites to control the configuration and altitude of the formation flying. Umair¹⁴⁾ designed the control strategy for Electromagnetic Satellite Formations in Near-Earth Orbit. Kwon¹⁵⁾ explored the applicability of EMFF for attitude and translation control of close proximity formation flying.

Inspired by the previous work, a new dynamical scenario was proposed by Peng,³⁾ where a charged spacecraft(follower) moves around a chief spacecraft which produces a rotating mag-

netic dipole. And the dipole is supposed to be produced by three concentric and orthogonal High Temperature Superconducting coils (HTS), thus in principle, any orientation of the dipole can be achieved by adjusting the charge in the three HTS wires.

While Paper³⁾ only considered the dipole to be pointing along the radial direction, this paper aims to extend the dynamical study of this model in such a way that three possible orientations of the dipole, that are normal, radial and tangential, are considered. However, our main attention lies on dynamical analysis, followed by the exploration of application potentials, therefore, we will not go into engineering details of the construction of HTS, or the strategy to charge electro-statically the satellites. And the numerical simulation will be based on the assumption that all the proposed magnetic field or charge-to-mass ratio can be satisfied, which although might be beyond the state-of-art technology, but can be realized in the near future.

The paper is organised as follows, in Sect. 2. the dynamical model is built, including the differential equations of motion and their symmetry properties. In Sect. 3. we study the equilibria and their stability behaviour. Sect. 4. explains the method to compute symmetric and asymmetric periodic orbits emanating from equilibria, and the numerical results are shown in Sect.5.. The applicability of this model is demonstrated in Sect. 6., by designing two formation flying configurations. Finally, Sect.7. contains a brief conclusion.

2. System model

2.1. Differential equations

We assume the mass of the follower is negligible compared with that of the leader, which is supposed to move in a high-Earth orbit (such as GEO), so the Lorentz force on the follower due to the geomagnetic field can be ignored. As a consequence, the follower is subjected to both gravitational force by the Earth and Lorentz forces by the artificial magnetic dipole. The coordinates system is chosen to be the local-vertical-local-horizontal (LVLH) coordinates, see Fig. 1. The origin is located at the chief, the x -axis (e_r) points from the Earth to the leader, the z -

[†]Corresponding author, Email: jyuan@nwpu.edu.cn

axis (e_n) is along the leader's orbital momentum vector, and the y -axis (e_r) completes the right-hand coordinate system.

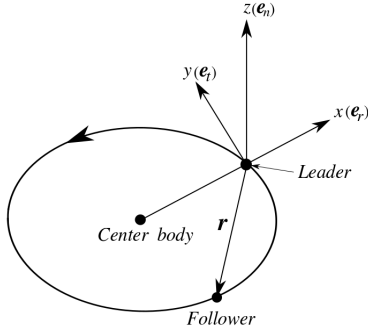


Fig. 1.: The Local Horizontal and Local Vertical Coordinate system.

The equations of motion can be expressed using the well-known Hill-Clohessy-Wiltshire equation:

$$\begin{aligned} \ddot{x} - 2n\dot{y} - 3n^2x &= f_x \\ \ddot{y} + 2n\dot{x} &= f_y \\ \ddot{z} + n^2z &= f_z \end{aligned} \quad (1)$$

where n is the mean motion of the chief's circular orbit around the Earth. $[f_x \ f_y \ f_z]^T$ are the three component of the acceleration force acting on the follower, in this study, they are modelled as Lorentz force f_L , and can be given by:

$$f_L = \frac{q}{m} \mathbf{v}_r \times \mathbf{B} = \frac{q}{m} \cdot (\dot{\mathbf{r}} - \omega_c \times \mathbf{r}) \times \mathbf{B} \quad (2)$$

where \mathbf{v}_r is the relative velocity of the charged follower with respect to the chief's rotating magnetic field, \mathbf{r} and $\dot{\mathbf{r}}$ are the follower's position and velocity relative to the chief. $\frac{q}{m}$ is the charge-to-mass ratio of the follower.

\mathbf{B} is the artificial magnetic field, which rotates in an angular velocity ω_c . By classical electrodynamics, \mathbf{B} is defined in terms of a vector potential \mathbf{A} :

$$\mathbf{B} = \nabla \times \mathbf{A} \quad (3)$$

where \mathbf{A} is given by :

$$\mathbf{A} = \frac{B_0}{r^2} (\hat{\mathbf{N}} \times \hat{\mathbf{r}}) = \frac{B_0}{r^2} [(z\hat{N}_y - y\hat{N}_z) \ (x\hat{N}_z - z\hat{N}_x) \ (y\hat{N}_x - x\hat{N}_y)]^T \quad (4)$$

where $\hat{\mathbf{r}} = [\hat{r}_x \ \hat{r}_y \ \hat{r}_z]^T$ is the unit vector of the spacecraft position, $\hat{\mathbf{N}} = [\hat{N}_x \ \hat{N}_y \ \hat{N}_z]^T$ is the dipole direction unit vector, and B_0 is the magnetic dipole moment (unit $Wb \cdot m$):¹⁵⁾

$$B_0 = \frac{\mu_0}{4\pi} n_c i_c \pi R_c^2 \quad (5)$$

where $\mu_0 = 4\pi \times 10^{-7} N/A^2$ is the vacuum permeability, n_c is the loops in the coil, i_c is the current flown in, and R_c is the radius.

Once the size of the coil is fixed, the magnetic dipole moment will be determined by the value of current passing through, which, according to the material of the coil and working temperature, will be limited by the current density of the coil. Nevertheless, we assume the coil can carry enough current to produce the required magnetic moment.

We assume that the magnetic dipole is rotating in the same direction as the dipole direction unit vector:

$$\omega_c = \omega_c [\hat{N}_x \ \hat{N}_y \ \hat{N}_z]^T \quad (6)$$

where ω_c is the dipole's rotational angular rate.

Substituting Eq.(3)-(6) into Eq.(2), we obtain

$$\begin{aligned} f_{Lx} &= \frac{q}{m} \frac{B_0}{r^3} \left[3(\hat{N} \cdot \hat{r})(y\hat{r}_z - z\hat{r}_y) - \omega_c(x\hat{N}_z - z\hat{N}_x)(3(\hat{N} \cdot \hat{r})\hat{r}_z - \hat{N}_z) \right] \\ &\quad + z\hat{N}_y - y\hat{N}_z + \omega_c(y\hat{N}_x - x\hat{N}_y)(3(\hat{N} \cdot \hat{r})\hat{r}_y - \hat{N}_y) \\ f_{Ly} &= \frac{q}{m} \frac{B_0}{r^3} \left[3(\hat{N} \cdot \hat{r})(z\hat{r}_x - x\hat{r}_z) - \omega_c(y\hat{N}_x - x\hat{N}_y)(3(\hat{N} \cdot \hat{r})\hat{r}_x - \hat{N}_x) \right] \\ &\quad + x\hat{N}_z - z\hat{N}_x + \omega_c(z\hat{N}_y - y\hat{N}_z)(3(\hat{N} \cdot \hat{r})\hat{r}_z - \hat{N}_z) \\ f_{Lz} &= \frac{q}{m} \frac{B_0}{r^3} \left[3(\hat{N} \cdot \hat{r})(x\hat{r}_y - y\hat{r}_x) - \omega_c(z\hat{N}_y - y\hat{N}_z)(3(\hat{N} \cdot \hat{r})\hat{r}_y - \hat{N}_y) \right] \\ &\quad + y\hat{N}_x - x\hat{N}_y + \omega_c(x\hat{N}_z - z\hat{N}_x)(3(\hat{N} \cdot \hat{r})\hat{r}_x - \hat{N}_x) \end{aligned} \quad (7)$$

We note that, in principle, the three orthogonal superconducting wires can produce magnetic field in any direction, but we will only consider the simplest cases, in which the orientation of the dipole points to three basic axes, as listed below:

1. **Normal case.** $N = [0 \ 0 \ 1]^T$, the dipole is parallel to e_n .
2. **Radial case.** $N = [1 \ 0 \ 0]^T$, the dipole is parallel to the chief's orbital radius vector e_r .
3. **Tangential case.** $N = [0 \ 1 \ 0]^T$, the dipole is parallel to e_t .

To simplify the equations of motion, we introduce the following unit sets for rescaling: time unit $\tau = n \cdot t$, length unit a that satisfies $a^3 = |B_0 \frac{q}{m} \frac{\omega_c}{n^2}| = |\frac{B_0}{n} \frac{q}{m} \frac{1}{\beta}|$ with $\beta = \frac{n}{\omega_c}$ as the angular quotient, and derivative with respect to τ , ($' = \frac{d}{d\tau} = n \cdot \dot{}$).

The radial case has been explored partly in,³⁾ including the eigenvalues, the stability characteristics. In this paper we will extend the research on this case, furthermore, we consider the other two cases with different orientations of the dipole, and do a deeper exploration on the dynamics and stability analysis for future potential in formation flying missions.

First we consider the case that the dipole direction unit vector is $N = [0 \ 0 \ \pm 1]^T$, which means the dipole axis is perpendicular to the chief's orbital plane, and we have

$$\begin{aligned} f_{Lx} &= \pm \frac{q}{m} \frac{B_0}{r^3} [-(x^2 + y^2 - 2z^2)y - 3yz\dot{z} \pm \omega_c x(x^2 + y^2 - 2z^2)] \\ f_{Ly} &= \pm \frac{q}{m} \frac{B_0}{r^3} [(x^2 + y^2 - 2z^2)\dot{x} + 3xz\dot{z} \pm \omega_c y(x^2 + y^2 - 2z^2)] \\ f_{Lz} &= \pm \frac{q}{m} \frac{B_0}{r^3} \cdot 3z[y\dot{x} - x\dot{y} \pm \omega_c(x^2 + y^2)] \end{aligned} \quad (8)$$

where ' \pm ' is the direction of the dipole with '+' refers to the positive z -axis, and '-' to the negative z -axis.

Since the charge q and angular rate ω_c can be both positive and negative real numbers, the same results can be obtained with different combination of positive or negative values of q and ω_c . We stress that the main attention is focused more on the qualitative study rather than too many duplicated computations, so only the case with '+' sign, in the normal case $N = [1 \ 0 \ 0]$, will be taken into consideration, the other cases with '-' can be studied using the same methodology.

After rescaling with the new unit sets, the equations of relative motion of the follower in normal case can be written as

$$\begin{aligned} X'' - 2Y' - 3X &= sgn \cdot \frac{-\beta(X^2 + Y^2 - 2Z^2)Y' - 3\beta YZZ' + X(X^2 + Y^2 - 2Z^2)}{R^5} \\ Y'' + 2X' &= sgn \cdot \frac{\beta(X^2 + Y^2 - 2Z^2)X' + 3\beta XZZ' + Y(X^2 + Y^2 - 2Z^2)}{R^5} \\ Z'' + Z &= sgn \cdot \frac{3Z[\beta YX' - \beta XY' + (X^2 + Y^2)]}{R^5} \end{aligned} \quad (9)$$

where $R = \sqrt{X^2 + Y^2 + Z^2}$, sgn is the sign of the charge on the follower, and so q/m . It is noted that, after the rescaling, only one system parameter remains, that is the angular quotient β .

The system admits a constant integral, referred as *Energy*,

$$H_n = 3X^2 - Z^2 - sgn \cdot \frac{2(X^2 + Y^2)}{R^3} - (X'^2 + Y'^2 + Z'^2) \quad (10)$$

For the **radial case**, we give the equations of relative motion in dimensionless unit, only for completeness of this paper,

$$\begin{aligned} X'' - 2Y' - 3X &= sgn \cdot \frac{3X[\beta ZY' - \beta YZ'(Y^2 + Z^2)]}{R^5} \\ Y'' + 2X' &= sgn \cdot \frac{-\beta(Y^2 + Z^2 - 2X^2)Z' - 3\beta XZX' + Y(Y^2 + Z^2 - 2X^2)}{R^5} \\ Z'' + Z &= sgn \cdot \frac{-\beta(Y^2 + Z^2 - 2X^2)Y' - 3\beta XYX' + Z(Y^2 + Z^2 - 2X^2)}{R^5} \end{aligned} \quad (11)$$

which also admits an integral constant, and is expressed as

$$H_r = 3X^2 - Z^2 - sgn \cdot \frac{2(Y^2 + Z^2)}{R^3} - (X'^2 + Y'^2 + Z'^2) \quad (12)$$

For the **tangential case**, the dimensionless equations of relative motion are given by:

$$\begin{aligned} X'' - 2Y' - 3X &= sgn \cdot \frac{\beta(X^2 + Z^2 - 2Y^2)Z' + 3\beta YZY' + X(X^2 + Z^2 - 2Y^2)}{R^5} \\ Y'' + 2X' &= sgn \cdot \frac{3Y[\beta XZ' - \beta ZX' + (X^2 + Z^2)]}{R^5} \\ Z'' + Z &= sgn \cdot \frac{-\beta(X^2 + Z^2 - 2Y^2)X' - 3\beta XYX' + Z(X^2 + Z^2 - 2Y^2)}{R^5} \end{aligned} \quad (13)$$

the corresponding energy is denoted as H_t , and is given by

$$H_t = 3X^2 - Z^2 - sgn \cdot \frac{2(X^2 + Z^2)}{R^3} - (X'^2 + Y'^2 + Z'^2) \quad (14)$$

To study the stability of the equilibria from dynamical point of view, it is convenient to write the equations of motion in general form of 1st-order differential equations. Denote the state vector as $\chi = (X, Y, Z, X', Y', Z')$, Eq. (9) can be rewritten as

$$\chi' = f(\chi) \quad (15)$$

where $\chi' = [X', Y', Z', X'', Y'', Z'']^T$ is the derivative of the state vector with respect to the time unit τ , $f = [f_1, f_2, f_3, f_4, f_5, f_6]^T$ is the vector field, and can be expressed as

$$\begin{aligned} f_1 &= X' \\ f_2 &= Y' \\ f_3 &= Z' \\ f_4 &= 3X + 2Y' + sgn \cdot \frac{-\beta(X^2 + Y^2 - 2Z^2)Y' - 3\beta YZZ' + X(X^2 + Y^2 - 2Z^2)}{R^5} \\ f_5 &= -2X' + sgn \cdot \frac{\beta(X^2 + Y^2 - 2Z^2)X' + 3\beta XZZ' + Y(X^2 + Y^2 - 2Z^2)}{R^5} \\ f_6 &= -Z + sgn \cdot \frac{3Z[\beta YX' - \beta XY' + (X^2 + Y^2)]}{R^5} \end{aligned} \quad (16)$$

where sgn , as referred before, is the sign of charge on the deputy. The 1st-order differential equations for radial and tangential cases can be written similarly.

2.2. Symmetries of the system model

The symmetries of the system will be explored by looking for transformations with a general form

$$P(t, x, y, z) := (Dt, Ax, By, Cz) \quad (17)$$

under which the coordinates of the image will be ($\bar{t} = Dt$, $\bar{x} = Ax$, $\bar{y} = By$, $\bar{z} = Cz$).

Provided that the image is also a solution, the equations of motion will be invariant under the transformation (17). By substituting the coordinates of the image into system equations, and setting the corresponding coefficients be identical to each other, the suitable solution sets for A, B, C and D can be obtained. For the normal case, we have: $A^2 = 1$, $B^2 = 1$, $C^2 = 1$, $D = AB$, the other two cases can be studied similarly.

The symmetry properties of the three cases, and the corresponding transformation sets are listed Table 1. For the normal

case, the symmetric elements include all possible cases: three basic axes, three basic planes and the origin. It indicates that once we obtain a basic trajectory, all the possible kinds of images also exist, and can be computed simply by the transformation specified by the corresponding set of (A, B, C, D) .

The symmetries ($I_n, II_n, VI_n, VII_n, I_r$ and I_t) with opposite time sense, as will be shown in Section 4., can be taken advantage to compute the symmetric periodic orbits when there is centre part around the equilibria, while the ones (III_n, IV_n and V_n and V_n, II_r, III_r and III_t), together with the original orbit, can provide perfect nominal orbits with same period for a formation fly configuration.

Table 1.: The symmetries exhibited by the equations of motion in the three cases, together with the corresponding transformation sets, symmetric elements and the time sense with respect to the original orbit.

Symmetric Type	(A, B, C, D)	Symmetric element	Sense
I_n	(1, -1, -1, -1)	X axis	Opposite
II_n	(-1, 1, -1, -1)	Y axis	Opposite
III_n	(-1, -1, 1, 1)	Z axis	Same
IV_n	(-1, -1, -1, 1)	Origin	Same
V_n	(1, 1, -1, 1)	X - Y plane	Same
VI_n	(-1, 1, 1, -1)	Y - Z plane	Opposite
VII_n	(1, -1, 1, -1)	X - Z plane	Opposite
I_r	(1, -1, 1, -1)	X - Z plane	Opposite
II_r	(-1, 1, -1, 1)	Y axis	Same
III_r	(-1, -1, -1, 1)	Origin	Same
I_t	(-1, 1, 1, -1)	Y - Z plane	Opposite
II_t	(1, -1, -1, 1)	X axis	Same
III_t	(-1, -1, -1, 1)	Origin	Same

3. Equilibrium points and their stability behaviour as a function of β

In this section, we are going to study the equilibria, and their stability behaviour as a function of an important parameter $\beta = \frac{n}{\omega_c}$, which stands for the angular quotient between the mean motion of the leader around the Earth and the dipole's rotational rate. By setting $X' = Y' = Z' = 0, X'' = Y'' = Z'' = 0$ in the equations of motion, we obtain the location of equilibria.

For the **normal case**, we obtain the rearranged equations from Eq(9) that are only dependent on the position coordinates (X, Y, Z) ,

$$\begin{aligned} 3X + sgn \cdot \frac{X(X^2 + Z^2 - 2Y^2)}{R^5} &= 0 \\ \frac{Y(X^2 + Y^2 - 2Z^2)}{R^5} &= 0 \\ -Z + sgn \cdot \frac{3Z(X^2 + Y^2)}{R^5} &= 0 \end{aligned} \quad (18)$$

Solving the above equations, we obtain the coordinates of ten equilibria, with different sign of charge, as listed in Table 2, together with the equilibria in other two cases., the location of them is displayed in Fig.2. In each case, they are classified into three kinds according to the energy level.

3.1. Linear stability of the equilibria

Next, the stability of the equilibria is explored using dynamical system theory by looking at their linear resembles in a local neighbourhood of the critical points, around which the lin-

Table 2.: The equilibrium points in the three cases,classified into 3 kinds according to the energy level

Index	X	Y	Z	$sgn(\frac{q}{m})$	H
1_n	0	$\pm\sqrt{2}Z$	$\pm(\frac{2}{3\sqrt{3}})^{\frac{1}{3}}$	+	-1.587401
2_n	$\pm(\frac{1}{12\sqrt{6}})^{\frac{1}{3}}$	0	$\pm\sqrt{5}X$	+	-0.629960
3_n	$\pm(\frac{1}{3})^{\frac{1}{3}}$	0	0	-	4.326748
1_r	0	0	± 1	+	-3
2_r	$\pm(\frac{2}{9\sqrt{3}})^{\frac{1}{3}}$	$\pm\sqrt{2}X$	0	-	2.289428
3_r	$\pm(\frac{1}{4\sqrt{2}})^{\frac{1}{3}}$	0	$\pm\sqrt{X}$	-	1.88988
1_t	0	0	± 1	+	-3
2_t	± 0.6934	0	0	-	4.326748
3_t	0	$\neq 0$	0	\pm	0

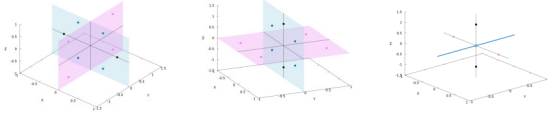


Fig. 2.: The location of equilibria in norma (left), radial (middle) and tangential case(right).

earised (first-order) equation can be written as,

$$\dot{\xi} = Df \cdot \xi \quad (19)$$

where ξ is the perturbation w.r.t. an equilibria χ_{eq} , Df is the Jacobi matrix, i.e., the derivative of f w.r.t. the state vector χ evaluated at the equilibrium point χ_{eq} , and

$$Df = \begin{bmatrix} 0 & 0 & 0 & 1 & 0 & 0 \\ 0 & 0 & 0 & 0 & 1 & 0 \\ 0 & 0 & 0 & 0 & 0 & 1 \\ f_{4X} & f_{4Y} & f_{4Z} & f_{4X'} & f_{4Y'} & f_{4Z'} \\ f_{5X} & f_{5Y} & f_{5Z} & f_{5X'} & f_{5Y'} & f_{5Z'} \\ f_{6X} & f_{6Y} & f_{6Z} & f_{6X'} & f_{6Y'} & f_{6Z'} \end{bmatrix} \quad (20)$$

where the second subscript stands for the variable w.r.t. which the derivative is computed. The first three rows of Df share the fixed form, while the last three rows can be expressed as

$$Df(4 : 6, :) = \frac{df_L}{d\chi} + \begin{bmatrix} 3 & 0 & 0 & 0 & 2 & 0 \\ 0 & 0 & 0 & -2 & 0 & 0 \\ 0 & 0 & -1 & 0 & 0 & 0 \end{bmatrix}$$

where $\frac{df_L}{d\chi}$ is the derivative of f_L w.r.t. the state vector χ .

For a given equilibrium point, the Jacobi matrix Df is only dependent on β , and due to the symmetry of the system, its characteristic polynomial can be expressed in a general form with only odd-order terms:

$$\lambda^6 + b\lambda^4 + c\lambda^2 + d = 0 \quad (21)$$

where b, c, d are either functions of β or constants. Denoting $\kappa = \lambda^2$, it can be further simplified into a cubic polynomial

$$\kappa^3 + b\kappa^2 + c\kappa + d = 0 \quad (22)$$

and its discriminant is given by¹⁸⁾

$$\Delta = 18bcd - 4b^3d + b^2c^2 - 4c^3 - 27d^2 \quad (23)$$

and the forms of roots can be classified according to the value of Δ : if $\Delta > 0$, we have three distinct real roots; and if $\Delta = 0$, we have multiple root and all of them are real; while with $\Delta < 0$, we have one real root and two complex conjugates.

As the square root of κ , the eigenvalues always come in pairs, i.e., for real ones we have $\pm\lambda$ with $\lambda \in \mathbb{R}$, while for complex ones we have conjugated pair $(\lambda, \bar{\lambda})$ with $\lambda \in \mathbb{C}$.

The eigenvalues of Df indicate the stability of the equilibrium at which it is evaluated.¹⁷⁾ Paper³⁾ provided the sufficient and necessary conditions for ten cases of equilibria according to the sign of Δ and b, c, d . In this paper, while following the rule in,³⁾ we draw our main attention on the qualitative results. Moreover, we explore numerically the evolution of all the eigenvalues as a function of β , to provide more straightforward information. With regard to the value of range of β , we would like the dipole rotates at a reasonably low rate, thus only small values are considered, for instance, $\beta \in [-40 : 40]$.

For equilibria of **Index** 1_n , we take the positive value for both Y and Z coordinate, and obtain the last three rows of Df

$$Df(4 : 6, :) = \begin{bmatrix} 3 & 0 & 0 & 0 & 2 & -\frac{\sqrt{2}}{2}\beta \\ 0 & \frac{2}{3} & -\frac{2\sqrt{2}}{3} & -2 & 0 & 0 \\ 0 & -\frac{2\sqrt{2}}{3} & -\frac{5}{3} & \frac{\sqrt{2}}{2}\beta & 0 & 0 \end{bmatrix} \quad (24)$$

The characteristic polynomial is of the same form for the four equilibria of this type, regardless of the signs, and is given by

$$\lambda^6 + (\frac{\beta^2}{2} + 2)\lambda^4 + \frac{-\beta^2 + 8\beta + 5}{3}\lambda^2 + 6 = 0 \quad (25)$$

Setting $\Delta = 0$, we get two roots $\beta_1 = -4.6645$ and $\beta_2 = 18.7239$. Despite the varying of β , the equilibria are always of type **saddle/saddle/centre**, which implies these equilibria are unstable, as well as the existence of one family of periodic orbits around each of the four equilibrium points. We note that $\beta \in [-4.6645, 18.7239]$, the saddle part is complex quadruple.

Table 3 lists the dimension of the manifolds associated to all kinds of equilibria in all the three case, as a function of β . Fig. 3 displays the behaviour of three kinds of eigenvalues in normal case (taking the one with positive coordinates as representation), in form of real and imaginary part as a function of β .

 Table 3.: The different cases of the dimension of manifolds associated with the equilibria of **index** $1_n, 1_r, 3_r$ and 1_t , as β varies the value

Equilibria	β	dim $W^{S,U}$	W^C
Index 1_n	$\beta \in (-\infty, -4.6645)$	2(real)	2
	$\beta \in (-4.6645, 18.7239)$	2(complex quadruple)	2
	$\beta \in (18.7239, \infty)$	2(real)	2
Index 1_r	$\beta \in (-\infty, -1.5604)$	2(real)	2
	$\beta \in (-1.5604, 1.5604)$	2(complex quadruple)	2
	$\beta \in (1.5604, \infty)$	2(real)	2
Index 3_r	$\beta \in (-\infty, -0.9516)$	0	6
	$\beta \in (-0.9516, 0.0732)$	2(complex quadruple)	2
	$\beta \in (0.0732, 1.5326)$	2(real)	2
	$\beta \in (1.5326, 3.4525)$	2(complex quadruple)	2
	$\beta \in (3.4525, \infty)$	0	6
Index 1_t	$\beta \in (-\infty, -4.3643)$	2(complex)	2
	$\beta \in (-4.3643, 4.3643)$	2(real)	2
	$\beta \in (4.3643, \infty)$	2(complex)	2

For the four equilibria of **index** 2_n , the characteristic polynomial is also identical, and is given by

$$\lambda^6 + (14\beta^2 + 12\beta + 8)\lambda^4 + \frac{-40\beta^2 + 80\beta - 1}{3}\lambda^2 - 60 = 0 \quad (26)$$

Since we have $\Delta < 0$ and $b = 14\beta^2 + 12\beta + 8 > 0$, $d = -60 < 0$ despite the value of β , there are always two pairs of imaginary eigenvalues and one pair of real eigenvalues. Therefore, the dimension of the associated stable and unstable manifolds is one, while that of the centre manifold is four. The corresponding two families of periodic orbits will be computed later.

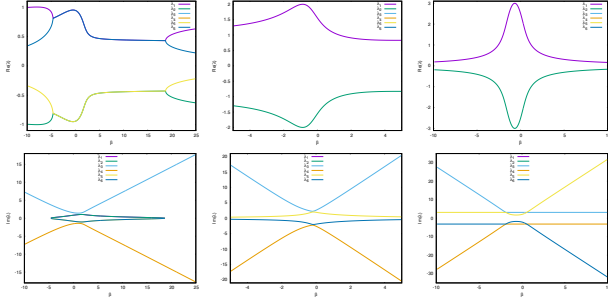


Fig. 3: As a function of β , the behaviour of eigenvalues associated to equilibria of index 1_n (left), 2_n (middle) and 3_n (right), in form of real (top) and imaginary (bottom) part, only the non-zero ones are plotted.

For the two equilibria of **index** 3_n , the characteristic polynomial are identical as

$$\lambda^6 + (9\beta^2 + 12\beta + 8)\lambda^4 + (90\beta^2 + 120\beta - 47)\lambda^2 - 270 = 0 \quad (27)$$

Since $\Delta > 0$ holds for all value of β except at $\beta_1 = -1.8823$ and $\beta_2 = 0.5490$, at which we have $\Delta = 0$, together with the fact that the two coefficient $b = 9\beta^2 + 12\beta + 8 > 0$ and $d = -270 < 0$. We have two couples of purely imaginary eigenvalues and one pair of real ones. Thus, the dimension of the associated stable and unstable manifold $W^{s,u}$ is one, while that of centre manifold is four, which embed two families of periodic orbits, the same pattern can be observed in Fig. 3, where one pair of pure imaginary eigenvalues remain constant, and the two pairs of purely imaginary eigenvalues collide when $\Delta = 0$.

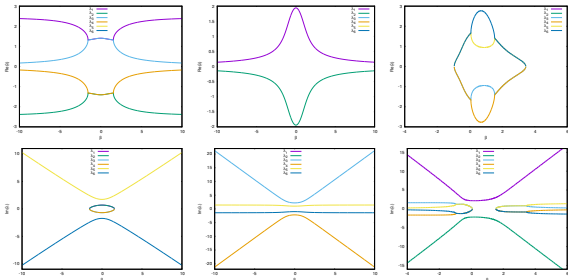


Fig. 4: In radial case, the behaviour of eigenvalues associated to the three kinds of equilibria(1_r , 2_r and 3_r from left to right) as a function of β , in top (real part) and in bottom (imaginary part)

The corresponding numerical results for radial and tangential cases are displayed in Fig.4 and 5, respectively. For the equilibria of **index** 2_r , the dimension of centre manifold is always four, which embeds two families of periodic orbits; while that of the stable and unstable manifold is one. We note that one pair of pure imaginary eigenvalues remain constant except around $\beta = 0$, see the middle plot of Fig.4.

The one attracts the most interests is **index** 3_r , since with $\beta \in (-\infty, -0.9516) \cup (3.4525, \infty)$, we have three families of periodic orbit, which of course, may provide plenty candidates for nominal orbits of future missions.

We note that the equilibria of **index** 3_r are quite specular, which include the whole Y - axis except the origin. We will not

discuss this kind of equilibria in the following section, since the energy $H_r = 0$, and they are not of much practical meaning.

The results for **index** 1_r and 2_r equilibria are show in Fig. 5. The patterns are similar to the first two kinds of equilibria in the radial case (Fig. 4), and are coherent with Table 2.

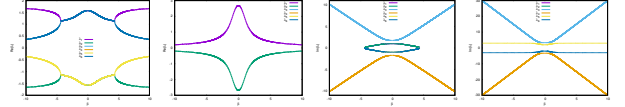


Fig. 5: As a function of β , the behaviour of the eigenvalues (real and imaginary part) associated to equilibria(left two **index** 1_r , and right two for **index** 2_r)

4. Computation of periodic orbits emanating from the equilibrium point

In this section, a systematic determination of the families of symmetric and asymmetric periodic orbits of the system defined by Eq.(9) and (11) has been done. The initial guess is given by the linearised differential equation around the equilibrium point being considered, a continuation method based on Adam predictor followed by a differential corrector procedure is applied to obtain the whole family of the periodic orbit; both use the linear variational equations.

The idea of computing one periodic orbit is as follows:¹⁹⁾ given an initial guess of the periodic orbit, we integrate up to a specific epoch or a specified crossing through a certain Poincaré section, then use differential correction procedure implemented by Newton Method, to satisfy the periodicity condition.

For a symmetric periodic orbit, we usually take the initial guess on the symmetric element (plane or axis) with initial velocity perpendicular to it, and the periodic condition is we return to the same reference plane or axis with perpendicular velocity after half (or a quarter) of the period (according the the symmetry type). While for an non-symmetric one, we have to integrate a full period until we return to the initial point.

4.1. Initial guess of the periodic orbit around the equilibrium points

The general solution of the differential equation of 6-degree-of-freedom like Eq.(19) can be written as $\mathbf{x}(t) = c_1 e^{\lambda_1 t} \mathbf{u}_1 + c_2 e^{\lambda_2 t} \mathbf{u}_2 + \dots + c_n e^{\lambda_n t} \mathbf{u}_n$, where λ_i ($i = 1 \sim 6$) are the eigenvalues and \mathbf{u}_i ($i = 1 \sim 6$) are the respective eigenvectors, c_i ($i = 1 \sim 6$) are constants.

Since we are interested only in the case that there exist periodic orbits, we will assume that at least two eigenvalues (in pair) are imaginary $\lambda_{1,2} = \pm \sqrt{-1} s = \pm is$, and set $c_3 = c_4 = c_5 = c_6 = 0$, in this way, we can write $\xi = c_1 e^{sit} \mathbf{v}_1 + c_2 e^{-sit} \bar{\mathbf{v}}_1$ where $\bar{\mathbf{v}}_1$ is the conjugate of \mathbf{v}_1 . If we denote $\mathbf{v}_1 = v_1^r + v_1^i$ ($v_1^r \in \mathbb{R}$, $v_1^i \in \mathbb{R}$), then ξ can be rewritten as

$$\begin{aligned} \xi &= c_1 (v_1^r \cos(st) + v_1^i \sin(st)) + c_2 (v_1^r \sin(st) - v_1^i \cos(st)) \\ &= A_\xi (v_1^r \cos(st - \phi) + v_1^i \sin(st - \phi)) \end{aligned} \quad (28)$$

where c_1, c_2 are arbitrary constants, $A_\xi = \sqrt{c_1^2 + c_2^2}$, $\sin \phi = \frac{c_2}{A_\xi}$.

The guess for the initial configuration of the periodic orbit is:

$$\mathbf{X}_0 = [X_1^0, X_2^0, X_3^0, X_4^0, X_5^0, X_6^0]^T = \mathbf{X}_{eq} + \epsilon \cdot \frac{\xi}{\|\xi\|} \quad (29)$$

where \mathbf{X}_{eq} is the state vector of the equilibrium point, and ϵ is a small distance along the solution ξ . In order not to violate

the linear assumption, we take the value to be 1×10^{-3} . If the dimension of the centre manifold is bigger than two, the other family of periodic orbit can be obtained in the same way by setting the coefficient $c_i = 0$, where i is the index of the coefficients that are not related to the considered centre part.

4.1.1. Initial guess for symmetric periodic orbits

According to Robin and Richardson,¹⁹⁾ the problem of the determination of symmetric periodic orbits can be reduced to find a set of initial conditions satisfying a mirror configuration, which, upon integration of the equations of motion up to a specified epoch, yields a second mirror configuration.

Assume the initial configuration is $(X^0, Y^0, Z^0, \dot{X}^0, \dot{Y}^0, \dot{Z}^0)$, and can be rewritten as $(X_1^0, X_2^0, X_3^0, X_4^0, X_5^0, X_6^0)$ with the component labelled in this way. We denote non-zero components as (X_i^0, X_j^0, X_k^0) with $i < j < k$, while the other components (X_l^0, X_m^0, X_n^0) with $l < m < n$ are zeros, such that we have $\{l, m, n\} \cap \{i, j, k\} = \{1, 2, 3, 4, 5, 6\}$. We summarise the different cases of the value of the index (i, j, k) , the corresponding symmetric element and the required type of mirror configurations, as seen in Table.4. *Case 1,2 and 3* exhibit plane-symmetry, while *case 4,5 and 6* possess axis-symmetry.

To obtain certain form of solution by Eq. (28), we can take $st + \phi = 0$ (or $pi/2$), to keep only the part of v_1^r or v_1^i that satisfies the corresponding initial configuration.

Table 4.: Cases for periodic orbits with different kinds of symmetry, and the required initial and final configuration

Case	Type of mirror configuration at initial/final epoch	Elapsed time	Symmetric element	(i, j, k)
1			X- axis	(1, 5, 6)
2	A / A	T/2	Y- axis	(2, 4, 6)
3			Z- axis	(3, 4, 5)
4			(Y - Z) plane	(2, 3, 4)
5	P / P	T/2	(X - Z) plane	(1, 3, 5)
6			(X - Y) plane	(1, 2, 6)

4.2. A differential corrector algorithm

Imposing the periodicity condition and taking the Poincaré section to be $X_l = 0$, we integrate from the initial configuration upon the first crossing through the Poincaré section, and arrive at the final configuration $(X_1^f, X_2^f, X_3^f, X_4^f, X_5^f, X_6^f)$, which is of the same form as the initial configuration, such that we have the zero components (X_i^f, X_j^f, X_k^f) and non-zero components (X_l^f, X_m^f, X_n^f) , with $\{l, m, n\} \cap \{i, j, k\} = \{1, 2, 3, 4, 5, 6\}$.

Taking *case 4* in Table 4 as an example, the system is symmetric with respect to X - Z plane, so we have $(i = 1, j = 3, k = 5)$, and initial configuration is in form of $[X^0, 0, Y^0, 0, \dot{Y}^0, 0]^T$. The problem can be simplified to a two-point boundary value problem, and the free parameter \mathbf{X} , is $\mathbf{X} = [X_i^0, X_j^0, X_k^0]^T$, with (i, j, k) as the indexes associated to the non-zero component in the initial condition, whose value can be specified by the last column in Table 4 according to the type of symmetry.

Since the final configuration is achieved by the crossing through the Poincaré section, $X_l^f = 0$ is satisfied by the algorithm. Due to the symmetry, to have a periodic orbit, it is sufficient that

$$F(\mathbf{X}) = \mathbf{0} \implies \begin{cases} F_1(X_i^0, X_j^0, X_k^0) = X_m^f = 0 \\ F_2(X_i^0, X_j^0, X_k^0) = X_n^f = 0 \end{cases} \quad (30)$$

where, (m, n) are the indexes of the zero components in the final condition.

By imposing the symmetry, the dimension of the problem to be solved by Newton method can be reduced by at least one half. With three unknowns (X_i^0, X_j^0, X_k^0) in the initial condition, and two Equations in (30) as the final constraints, we apply the modified Newton Method to refine the periodic orbit. The least-square solution can be expressed iteratively as

$$\begin{aligned} \mathbf{X}_K &= \mathbf{X}_{K-1} + \delta \mathbf{X}_{K-1} \\ \delta \mathbf{X}_{K-1} &= -G^T (GG^T)^{-1} \cdot \mathbf{F}(\mathbf{X}_{K-1}) \end{aligned} \quad (31)$$

where, $K = 1, 2, \dots, n$ is the step of iteration, G is the Jacobian matrix of \mathbf{F} with respect to (x_i^0, x_j^0, x_k^0) , and is given by

$$G = \begin{bmatrix} \Phi(m, i) & \Phi(m, j) & \Phi(m, k) \\ \Phi(n, i) & \Phi(n, j) & \Phi(n, k) \end{bmatrix} - \frac{1}{\dot{X}_l^f} \begin{bmatrix} \ddot{X}_m^f \\ \ddot{X}_n^f \end{bmatrix} \begin{bmatrix} \Phi(l, i) & \Phi(l, j) & \Phi(l, k) \end{bmatrix}$$

where, Φ is the 6×6 state transit matrix, which satisfies $\dot{\Phi} = DX \cdot \Phi$, $DX = \frac{\partial \mathbf{f}}{\partial \mathbf{X}}$ with the initial value $\Phi_0 = \mathbf{I}_{6 \times 6}$ and DX is the differential of the vector field with respect to the state vector.

Repeat the correction process until the constraints are met within error tolerance 1×10^{-11} , the same value is used for the determination of Poincaré section crossing. Finally we get the period: $T_p = 2t_f$, where t_f is the time elapsed from the initial point to the first intersection with Poincaré section.

4.3. The continuation method

Eq. (30) describes the characteristic curve of the family in the three-dimensional space of initial conditions. The determination of the characteristic curve can be done using a continuation method and the arc-parameter, s , of the curve. It is easy to verify that the characteristic curve of initial conditions $(X_i(s), X_j(s), X_k(s))$ fulfils

$$\frac{dX_i}{ds} = \frac{A_1}{A_0}, \quad \frac{dX_j}{ds} = \frac{A_2}{A_0}, \quad \frac{dX_k}{ds} = \frac{A_3}{A_0} \quad (32)$$

where $A_0 = (A_1^2 + A_2^2 + A_3^2)^{1/2}$, $A_1 = (F_{X_j}^1 F_{X_k}^2 - F_{X_k}^1 F_{X_j}^2)$, $A_2 = -(F_{X_i}^1 F_{X_k}^2 - F_{X_k}^1 F_{X_i}^2)$, $A_3 = -(F_{X_i}^1 F_{X_j}^2 - F_{X_j}^1 F_{X_i}^2)$. And $F_{X_i(X_j, X_k)}^{1(2)}$ is the partial derivative of $F^{1(2)}$ with respect to $X_i(X_j, X_k)$.

The integration of Eq. (32) is done using an Adams predictor method of one, two, three or four steps, depending on the number of points on the curve available.¹⁷⁾ If we suppose that some points $X_1, X_2, \dots, X_K, K > 1$ on the characteristic curve are known, the Adams method gives a new point X_{K+1}^0 near the curve. The point X_{K+1}^0 must be refined in order to obtain a new p.o. X_{K+1} , using the differential corrector.

With regard to the step size Δs to be used along the continuous arc, we follow the strategy of an automatic control explained in.²⁰⁾ Δs should be not too big to guarantee a smooth curve, either too small to make the continuation fast.

4.4. Computation of asymmetric periodic orbits

It happens that the centre-eigenvector does not satisfy any symmetric configuration in Table 4, then the above refinement strategy for will no longer be suitable. We can adjust the periodicity condition to be returning to the same initial point after a full period, the corrector and continuation method being adjusted correspondingly. In principle, we have 7 unknowns $\mathbf{X} = [X^0, Y^0, Z^0, X^0, Y^0, Z^0, T]^T$ (6 state vector + period), and 6 equations $\mathbf{X}^f - \mathbf{X}^0 = \mathbf{0}$.

To improve convergence we add one more equation to fix one coordinate of the initial configuration, for example, $Y^0 = 0$. Consider that the energy is preserved during the integration, we can eliminate one of the constraint on final state, i.e., $Z^f - Z^0 = 0$. As a consequence, we have a system of 6 unknowns and 5 equations to solve. The Jacobi matrix G in Eq. (31) is a 6×5 matrix, and is given by $G = \Phi - I$, and eliminating the 6-th row to remove constraint $Z^f - Z^0 = 0$, and the second column to remove the correction on initial component Y^0 .

For the continuation procedure, the key point is to compute the vector field \mathbf{v} along the characteristic curve, as in Eq. (32), which is also the kernel of G , can be expressed by

$$\mathbf{v} = [A_1, A_2, \dots, A_6]^T, i = 1, \dots, 6, \mathbf{v} \in \ker(G) \quad (33)$$

where A_i is the submatrix of G by eliminating the i - column of G , and \mathbf{v} is then normalized $\mathbf{v} = \frac{\mathbf{v}}{\|\mathbf{v}\|}$ to obtain a unit vector..

4.5. Linear stability of periodic orbit

The linear stability of periodic orbits can be approximated by the Monodromy matrix $M = \phi_{T_p}(\chi)$, that is the variational matrix after one full period T_p . There are some basic properties of the eigenvalues of M , the so-called characteristic multiplier:¹⁷⁾ the multipliers come in couples, if λ is an eigenvalue, then $1/\lambda, \bar{\lambda}$ and $1/\bar{\lambda}$ are also eigenvalues with the same multiplicity; $\det(M) = 1$, so 0 is not a multiplier, and 1 is one with at least multiplicity 2.

Since we have three couples of multipliers, denoted as $(\lambda_1, \lambda_1^{-1}), (\lambda_2, \lambda_2^{-1})$ and $(\lambda_3 = \lambda_3^{-1} = 1)$. The stability of periodic orbits can be clarified by checking the value of trace $Tr_i = \lambda_i + 1/\lambda_i, i = 1, 2$. For simplicity, we will always assume $Re(\lambda_i) > Re(\lambda_i^{-1})$, and denote $\lambda = a + bi$. We follow the rules in Paper¹⁷⁾ to study the stability of one periodic orbit, which can be concluded briefly as: the periodic orbit is unstable when $|Tr| > 2$, and stable with $|Tr| < 2$, when the $Tr = \pm 2$ always imply a bifurcation or the termination of the family.

5. Numerical results of periodic orbits

In this section, we compute all the families of periodic orbits that emerge from the centre manifold, if exists, around the computed equilibria, and study the stability behaviour, as well as the termination of each family.

5.1. Around the equilibria of index 1_n

For all value of β , the four equilibria of index 1_n are always of type **saddle/ saddle/centre**, only one family of periodic orbits exists. Type VI symmetry is considered since equilibria 1_n are on $(Y - Z)$ plane. We consider only the equilibrium point with $Y > 0, Z > 0$, the cases for other three can be obtained by imposing symmetry of type III_n, IV_n and V_n, respectively.

Taking $\beta = 2$ as example, the eigenvalues are $(\pm 0.6509, \pm 1.0291i, \pm 1.6520i)$, the eigenvector associated to the centre part $\pm 1.6520i$ is $\omega^c = \omega_r^c \pm \omega_i^c$ with $\omega_r^c = [0.2477, 0, 0, -0.1968, 0.7250]^T, \omega_i^c = [0, 0.1191, -0.4389, 0.4092, 0, 0]^T$. Since ω_i^c satisfies a P configuration with indexes of non-zero components as $(i = 2, j = 3, k = 4)$, it is taken as ϵ for the guess of initial mirror configuration in Eq. (28), the periodic orbit obtained is shown in Fig. 6, as well as the continuation of this family.

A connection is observed between two equilibrium points of **index 1_n** located at $(0, \sqrt{2}Z, (\frac{2}{3\sqrt{3}})^{\frac{1}{3}})$ and $(0, -\sqrt{2}Z, (\frac{2}{3\sqrt{3}})^{\frac{1}{3}})$, and the family of periodic orbits terminates at the second one.

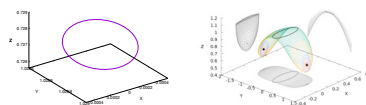


Fig. 6.: With $\beta = 2$, left: the periodic orbit emanating from equilibria 1_n ($X > 0, Z > 0$), associated to $\lambda = \pm 1.6520i$. right: the continuation family in 3D view (colored) with the three 2D projections (gray), a connection is detected between two symmetric equilibria (black points).

We display the characteristic curve (energy vs. period) and the trace as a function of energy for the stability analysis, see Fig.7. The periodic orbits and the characteristic curve are plot in different colors according to their topology type. Two bifurcations are detected when the real part of the trace crosses $Re(Tr) = -2$, demonstrated as vertical dashes line. For energy level below $H_n = -1.8491$, the orbits (in green) is stable and totally elliptic. A saddle-node bifurcation occurs at energy $H_n = -1.8491$, after which the orbits (orange) become unstable, and transits to hyperbolic \times elliptic. A second saddle-node bifurcation happens at energy level $H_n = -1.6147$, after which the orbits are hyperbolic. For the right-most small segment (red) in bottom-left plot in Fig. 7, where the energy $H_n > -1.6$ and the two traces merge in real part, that is because we have the multiplier as complex quadrupole in form of $(a \pm bi, 1/(a \pm bi))$, which makes the traces complex conjugate.

Due to type VII symmetry and the fact that those two equilibria are symmetric with respect to $(X - Z)$ plane, the left branch of this family, the ones in the left of the middle orbit (green) can be seen as the type VII images of the right branch (in the right of the middle green periodic orbit). As a consequence, the very periodic orbit in the middle is symmetric with respect to both $(X - Z)$ plane and $(Y - Z)$ plane, and is "almost" parallel to $X - Y$ plane, with the maximum Z - amplitude in order of 1×10^{-5} , which proves perfect nominal orbits for a displaced observation mission, a two-satellite configuration is to be studied later.

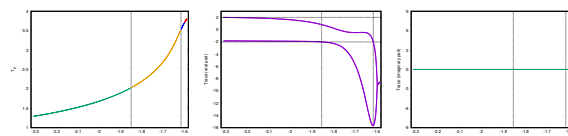


Fig. 7.: The continuation family of periodic orbits associated to Fig. 6. Left: the characteristic (energy vs period) curve; Different colors indicate different topology types, with stable ones in green and unstable ones for other colors, and the trace as a function of energy, in real (middle) and imaginary (right) part, the intersections with dashed vertical lines imply bifurcations.

The connection happens for the other two equilibria $(0, \pm \sqrt{2}Z, -(\frac{2}{3\sqrt{3}})^{\frac{1}{3}})$, see Fig. 9(left). This holds for other values of $\beta > 0$, that is when the dipole rotates in the same sense as the chief's motion around the Earth.

However, when the dipole rotates oppositely as the chief's motion around the Earth, that is $\beta < 0$, we observe a different phenomena. The connection between two equilibria disappears, instead, the period tends to π as the energy decreases. An example with $\beta = -2$ is shown in Fig.8. It can be seen that the Z -amplitude becomes rather large while the period tends to a limit of π . The family is unstable, although the topology type of the multiplier has three transitions between real and complex space.

The isolation between two families of periodic orbit emerging from different equilibria is displayed in Fig. 9(right).

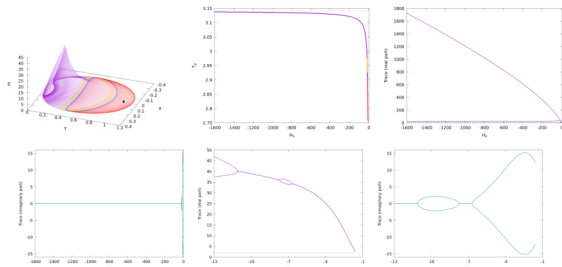


Fig. 8.: With $\beta = -2$, the family of periodic orbit emerging from equilibrium point 1_n ($Y > 0, Z > 0$). Top left: the periodic orbits, all of them are unstable, different colors are of different topology types; Top middle: the characteristic (energy vs period) curve; The real part (top right) and imaginary part(bottom left) of the trace as a function of energy H_n , together with a magnification(real part in bottom middle and imaginary part in bottom right) within the region $H_n \in [-13 : -1]$.

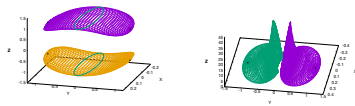


Fig. 9.: The two connections between equilibria of index 1_n with $\beta = 2$ (left); and two isolated families of periodic orbits with $\beta = -2$ (right).

By applying symmetry of type III_n and V_n , all families of periodic orbits emanating from equilibria 1_n can be obtained, see Fig. 9. We note that, the other values of β provides qualitatively the same results according to the sign of β . The periodic orbits associated to other equilibria of the same kind, if not shown, can be obtained by imposing the respective symmetry.

5.2. Around the equilibria of index 2_n

The centre manifold associated to equilibria 2_n is of dimension 4, which always embeds two families of periodic orbits. The results for $\beta = 2$ are shown in Fig. 10 and 11.

The first family(purple) degenerates to another equilibria, while the second one (green) terminates when the complex conjugate multipliers turn to one of multiplicity 2, which makes the multiplier 1 in total of multiplicity 4. For both families, a monotonous dependence between energy and period is demonstrated, and all the orbits are of type hyperbolic \times elliptic.

The periodic orbits associated to other three equilibria can be obtained by applying symmetry III_n, IV_n and V_n , see Fig. 12 (right). We stress that, for this kind of equilibria, there is no qualitative difference with other values of β . From now on, for the simplicity without losing generality, we will only display the results for one equilibria point, at one or several values of β , if there is no qualitative difference.

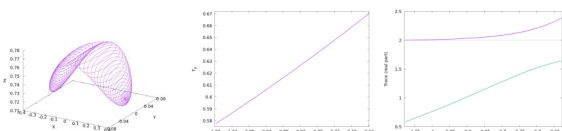


Fig. 10.: The first family of periodic orbits emanating from equilibrium point of type 2_n ($X > 0, Z > 0$) with $\beta = 2$, the periodic orbit(left), the period-energy curve(middle) and the trace (real curve) (right).

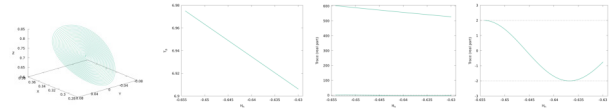


Fig. 11.: The second family of periodic orbits associated to equilibrium point of type 2_n ($X > 0, Z > 0$), from left to right: the periodic orbit, the characteristic curve, the trace(real curve, with the magnification (rightmost) of the region before termination).

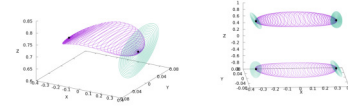


Fig. 12.: With $\beta = 2$. Left: the two families associated to equilibria of type 2_n with ($X > 0, Z > 0$). Right: all families of periodic orbits emerging from this kind of equilibria obtained by imposing symmetry III_n, IV_n and V_n .

5.3. Around the equilibria of index 3_n

The centre manifold around equilibria of index 3_n is of dimension four, and contains two families of periodic orbits. In this case, the qualitative behaviour of the periodic orbits is independent of the sign of β . The eigenvalues are of form $(\pm\lambda_1 i, \pm\lambda_2 i, \pm\lambda_3)$ with $\lambda_{1,2,3} \in \mathbb{R}$.

Taking $\beta = 2$ for demonstration purpose, we obtain $\lambda_1 = 7.6460, \lambda_2 = 3.1623, \lambda_3 = 0.6796$. The first family associated to λ_1 is planar, see Fig. 13. A saddle-node bifurcation is detected at $H_n = 3.8272$, before which the orbits are of type hyperbolic \times elliptic, and transits to totally elliptic afterwards.

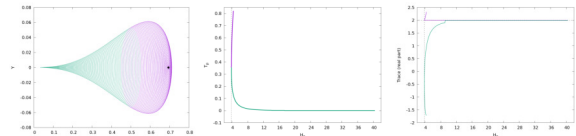


Fig. 13.: The planar family emanating from type 3_n ($X > 0$) equilibria, left: the periodic orbits (stable in green and unstable in purple). Middle: the characteristic curve. Right: the trace(real curve, a bifurcation occurs at the vertical dashed line

For the second family associated to $\lambda_2 = 3.1623$, it degenerates into a planar orbits at $H_n = 3.868084$ (marked as A), see Fig. (14), along with the characteristic curve and the trace curve. The shape and evolution of periodic orbits and their stability behaviour in this family are rather complicated, several bifurcations are detected, which will be studied in detail.

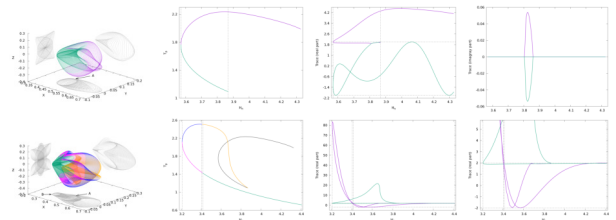


Fig. 14.: The second family of periodic orbits associated to $\lambda_2 = 3.1623$ before the first bifurcation(top) and after the first bifurcation(bottom). From left to right we have: the 3D view (stable in green) and the three 2D projections(gray), the characteristic curve, the trace curve (tr_1 in purple and tr_2 in green) in real part and imaginary part.

If we proceed the continuation along the new branch at the degenerated point, we obtain another family, see Fig. 14 (bottom). Three bifurcations are detected when the trace curve cross $Tr = 2$ line, indicated as vertical dashed line. A node-saddle bifurcation is detected at $H_n = 3.56957$, the evolution of the size and shape of the orbits before and after the first bifurcation is displayed in Fig. 15, the loops within one revolution change from two to six. An overlap of two families of periodic orbits shows clearly two intersections, see Fig.16 (left), which corresponds to A and B in Fig.14.

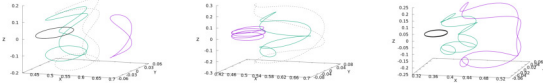


Fig. 15.: Orbit samples with different loops before(left) and after (middle) the first bifurcation, and the ones after the second bifurcation(right), the evolution goes in order purple \rightarrow green \rightarrow dashed black (bifurcation point). The solid black orbits (if exists) are the termination point.

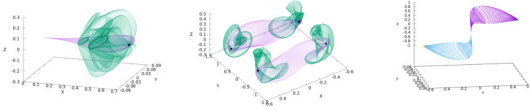


Fig. 16.: Left: the overlap of two families of periodic orbits emanating from equilibrium point 3_r ($X > 0$), two intersections (black curves) are detected. Middle: the two families of periodic orbits in radial case with $\beta = 2$, around the equilibria of index 3_r , with two connections detected. Right: A connection between two equilibria 3_r , the intersection occurs at the origin.

5.4. Around equilibria of Index 1_r

For this type of equilibria, the centre manifold is of dimension 2, the embedded family of periodic orbits with $\beta = 2$ is displayed in Fig. 17. Similar to the family shown in Fig.8, the size of the orbit grow to be very large as the energy decreases, but the period tends to an upper limit of π . For demonstration purpose, we only display a small portion of the trace curve when the energy is above -3 , afterwards the same trend continues while the value of the trace tend to $-\infty$.

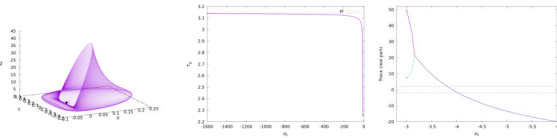


Fig. 17.: The family of periodic orbits emanating from equilibria 1_r ($X, Y > 0$). Left: periodic orbits, middle: characteristic curve, right: trace (real) curve.

5.5. Around equilibria of Index 2_r

We always have two families of periodic orbits emanating from each equilibria 2_r , since the centre manifold is of dimension 4 regardless of the value of β . Fig. 18 displays the result for $\beta = 2$, and the eigenvalues are ($\lambda_1 = \pm 4.3528i, \lambda_2 = \pm 1.2784i, \lambda_3 = \pm 0.7624$).

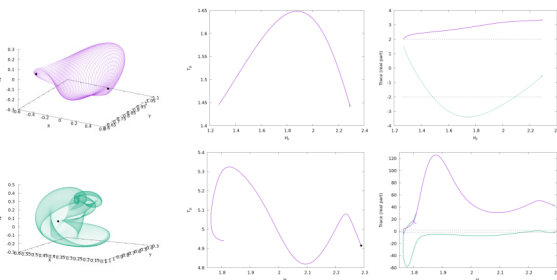


Fig. 18.: The two family of periodic orbits emanating from equilibria 2_r ($X > 0, Y > 0$). The family associated to $\lambda_1 = \pm 4.3528i$ (top) degenerates to to another equilibria ($X < 0, Y > 0$), and second is to $\lambda_2 = \pm 1.2784i$ (bottom). Left: periodic orbits, middle: characteristic curve, right: trace (real) curve.

The periodic orbits around the other two equilibria can be obtained by apply type I_r, II_r and III_r , see Fig.16(middle).

5.6. Around equilibria of index 3_r

For this kind of equilibria, we have three pairs of imaginary eigenvalues, and three families of periodic orbits. Take $\beta = 6$ as example, and consider the two symmetric equilibria with $X = Z, X > 0$, we obtain the eigenvalues of the Jacobi matrix

($\pm 16.912393i, \pm 1.376370i, \pm 0.257753i$). The numerical results of periodic orbits and their stability behaviour are shown in Fig. 19.

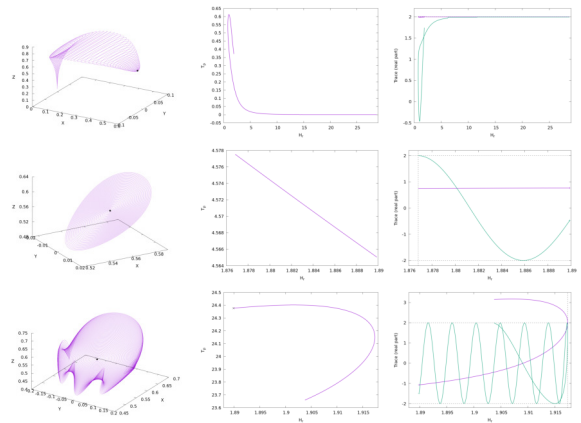


Fig. 19.: Three families of periodic orbits emanating from equilibria of index 1_r with $X = Z$, associated to λ_1, λ_2 and λ_3 from top to bottom. left: periodic orbits, middle: characteristic curve, right: trace curve.

A connection between two families of periodic orbits has been detected see Fig.16(right), which belongs to the *top left* plot in Fig. 19 and its image symmetric w.r.t. the origin. For this kind of equilibria, the two with $X = Z$ have the same characteristic polynomial and the stability behaviour while the other two with $X = -Z$ possess different one, see Fig. 20.

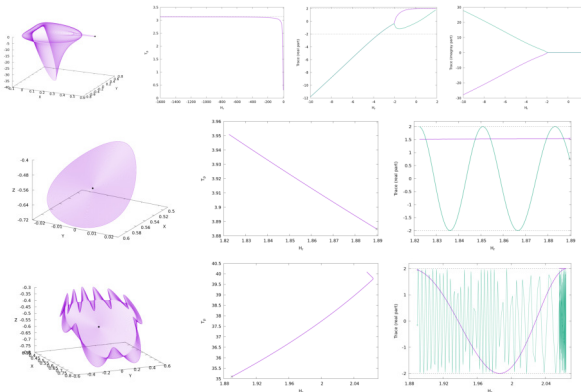


Fig. 20.: The family emanating from equilibria 1_r with $X = -Z$, associated to λ_1 (top), to λ_2 (middle) and to λ_3 (bottom). From left to right: periodic orbits, characteristic curve, and trace curve in real part (and imaginary part if its not equal to 0)

6. Suitable Formation flying configuration design

In this section, we will propose several formation flying configurations using the periodic orbits computed as the nominal orbits. With the most kinds (seven) of symmetry, the normal case draws our main attention, in which the magnetic field B is perpendicular to the orbital plane. Considering the fact that in some symmetries (types I_n, II_n, VI_n and VII_n) the sense of orbit is reversed, which will destroy the formation configuration as it evolves with time, we only apply the others (types III_n, IV_n and V_n) in which the sense is preserved. These last three ones will be, in principle, more suitable for a formation.

Using the two green periodic orbits in Fig. 12 that are "almost" parallel to $(X - Y)$ plane, we design a two-satellite configuration, with one satellite placed on one orbit. For missions that require the distance between two satellites to be constant, these two periodic orbits provide perfect nominal orbits. We

display the configuration at four epochs during one period, see Fig. 21, the sense of satellites' motion is counter-clockwise.

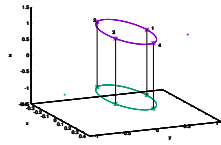


Fig. 21.: The configuration of two-satellite at several epoches $T/4*(i-1)$, ($i = 1, 2, 3, 4$) where T is the period. In black are the segments of the configuration, marked as stars are the spacecrafts, and in colored (purple and green) lines are the two periodic orbits where the spacecrafts are located on. The points are two equilibria of **index** 1_n



Fig. 22.: The configuration at several epoches $t_i = T/4*(i-1)$, ($i = 1, 2, 3, 4$) from left to right, where T is the period. In black are the segments of the configuration, marked as points are the spacecrafts, and in colored (green, orange, blue and purple) lines are the four periodic orbits where the spacecrafts are located on. The four round points are the four symmetric equilibria of **index** 2_n .

Another possible configuration is to place four satellites on four symmetric periodic orbits. We consider the second family associated to equilibria of index 2_n as shown in Fig.9(green). Note that these orbits are obtained using the symmetries of type III_n, IV_n and V_n .

The above configurations are designed based on the assumption that all the satellites are identical in mass and charge, and so $\frac{q}{m}$. If we adjust the charge on one or more satellites through an electron beam, new periodic orbits of same period, but in different size can be obtained. As a consequence, once a simple configuration is designed in non-dimensional unit, a same configuration of different size or a combination based on original one of any number, in any size, can be easily obtained.

7. Conclusion

In this paper, we have studied the relative motion of a charged spacecraft around any chief spacecraft, when the chief is orbiting around the Earth, with a rotating artificial magnetic dipole deployed on. Three general cases of the orientation of the dipole have been considered. From the dynamical system theory point of view, we computed the equilibria and their stability behaviour with respect to parameter β . The phase space around each equilibria is explore in such a way that different families of periodic orbits, their continuation, bifurcation, linear stability and termination are also studied. Two formation flying configurations are designed using the symmetric periodic orbits obtained, which proves the great potential of the plenty periodic orbits as the nominal orbits for formation flying missions.

Acknowledgments

Y.C. thanks the support of Doctorate Foundation of Northwestern Polytechnical University and the Chinese Scholarship Council. G.G. thanks the Catalan grant government J.J.M.

thanks MINECO-FEDER for the grant MTM2015-65715-P and the Catalan government for the grant 2014SGR504. for the grant 2014 SGR 1145, and MINECO-FEDER for the grant MTM2013-41168-P.

References

- Hough, M. E.: Lorentz Force Perturbations of A Charged Ballistic Missile. *Proceedings of the AIAA Guidance and Control Conference*, AIAA-1982-1549, San Diego, CA, 1982.
- Vokrouhlicky, D. : The Geomagnetic Effects on the Motion of Electrically Charged Artificial Satellite. *Celestial Mechanics and Dynamical Astronomy*, **46**(1989), pp. 85–104.
- Peng, C: Relative Orbital Motion of a Charged Object near a Spaceborne Radially-Directed Rotating Magnetic Dipole, *66th International Astronautical Congress*, Jerusalem, 2015.
- Peck, M. A.: Prospects and Challenges for Lorentz-Augmented Orbits. *Proceedings of the AIAA Guidance, Navigation, and Control Conference*, AIAA- 2005-5995, San Francisco, CA, August 2005.
- Schaffer, L., Burns, J. A.: Charged Dust in Planetary Magnetospheres: Hamiltonian Dynamics and Numerical Simulations for Highly Charged Grains. *Journal of Geophysical Research*, **99**(1994), pp. 17211–17223.
- Streetman, B., Peck M.A.: New Synchronous Orbits Using the Geomagnetic Lorentz Force. *Journal of Guidance, Control and Dynamics*, **30**(2007), pp. 1677–1690.
- Peck, M. A., Streetman, B., Saaj, C. M., and Lappas, V.: Spacecraft Formation Flying Using Lorentz Forces. *Journal of British Interplanetary Society*, **60**(2007), pp. 263–267.
- Atchison, J., Peck, M.: Lorentz-Augmented Jovian Orbit Insertion. *Journal of Guidance, Control, and Dynamics*, **32**(2009), pp. 418–425.
- Streetman, B., Peck, M.: Gravity-Assist Maneuvers Augmented by the Lorentz Force. *Journal of Guidance, Control, and Dynamics*, **32**(2009), pp. 1639–1647.
- Sobiesiak, L. A., Damaren, C. J.: Controllability of Lorentz-Augmented Spacecraft Formations. *Journal of Guidance Control and Dynamics*, **38**(2015), pp. 2188–2195.
- Streetman, B., Peck, M.A.: A General Bang-Bang Control Method for Lorentz Augmented Orbits. *AAS Spaceflight Mechanics Meeting*, AAS Paper 08-111, Galveston, Texas, 2008.
- King, L. B., Parker, G. G., Deshmukh, S., Chong, J.-H.: Study of Interspacecraft Coulomb Forces and Implications for Formation Flying. *Journal of Propulsion and Power*, **19**, (2003), pp. 497–505.
- Kong, E., Kwon, D., Schweighart, S., Elias, L., Sedwick, R., and Miller, D.: Electromagnetic Formation Flight for Multi-Satellite Arrays. *Journal of Spacecraft and Rockets*, **41**(2004), pp. 659–666.
- Umair A., Miller, D.W., Ramirez, J.L: Control of Electromagnetic Satellite Formations in Near-Earth Orbit. *Journal of Guidance, Control and Dynamics*, **33**(2010), pp. 1883–1891.
- Kwon D W.: Propellantless formation flight applications using electromagnetic satellite formations. *Acta Astronautica*, **67**(2010), pp. 1189–1201.
- Tsujii, S., Bando, M., Yamakawa, H.: Spacecraft formation flying dynamics and control using the geomagnetic Lorentz force. *Journal of Guidance, Control, and Dynamics*, **36**(2012), pp. 136–148.
- Gómez G., Mondelo J. M. The dynamics around the collinear equilibrium points of the RTBP. *Physica D: Nonlinear Phenomena*, **157**(2001), pp. 283–321.
- Irving R.S.: *Integers, Polynomials, and Rings*. Springer, 2004.
- Robin I. A., Markellos V. V.: Numerical determination of three-dimensional periodic orbits generated from vertical self-resonant satellite orbits. *Celestial Mechanics*, **21**(1980), pp. 395–434.
- Simó C.: On the analytical and numerical approximation of invariant manifolds. In D. Benest and C. Froeshl, editors, *Modern methods in Celestial Mechanics*, pages 285C330. Editions Frontiers, 1990.